https://doi.org/10.15407/ufm.27.01.025

A.B. SHEVCHENKO [1,2,*], A.V. MINITSKYI [3,],**
O.V. OLIINYK [1,*], and M.Yu. BARABASH [2,3,****]**

[1] G.V. Kurdyumov Institute for Metal Physics of the N.A.S. of Ukraine,
36 Academician Vernadsky Blvd., UA-03142 Kyiv, Ukraine

[2] Technical Centre of the N.A.S. of Ukraine,
13 Pokrovska Str., UA-04070 Kyiv, Ukraine

[3] National Technical University of Ukraine
'Igor Sikorsky Kyiv Polytechnic Institute',
37 Beresteiskyi Ave., UA-03056 Kyiv, Ukraine

* andborshev@ukr.net, ** aminitsky@gmail.com,
*** neutrino@ukr.net, **** mbarabash@nasu.kiev.ua

BLOCH POINT IN THE DOMAIN WALL OF A CYLINDRICAL FERROMAGNETIC NANOWIRE AS A HARMONIC OSCILLATOR: CLASSICAL AND QUANTUM PROPERTIES

The oscillatory properties (both classical and quantum ones) of the Bloch point (BP) in the domain wall of a cylindrical ferromagnetic nanowire are reviewed. Based on the presented results, it is concluded that BP can be considered as a harmonic oscillator. In this case, the quantum oscillations of BP are a type of magnetic macroscopic quantum effect [1] that occurs in nickel and iron nanowires at liquid-helium temperatures. It is shown the transformation of the BP wave packet into beat that ensures the transfer of the quantum-oscillator energy. The presented results are of particular interest in the context of the development of up-to-date nanotechnologies based on the physical properties of cylindrical ferromagnetic nanowires, the magnetic structure of which is characterised by the domain wall with BP.

Keywords: cylindrical ferromagnetic nanowire, domain wall, Bloch point, harmonic oscillations, wave packet, beat.

Citation: A.B. Shevchenko, A.V. Minitskyi, O.V. Oliinyk, and M.Yu. Barabash, Bloch Point in the Domain Wall of a Cylindrical Ferromagnetic Nanowire as a Harmonic Oscillator: Classical and Quantum Properties, *Progress in Physics of Metals*, **27**, No. 1: 25–49 (2026)

1. Introduction

The study of the physical properties of nanowires is one of the priority tasks in nanoscale science. Due to their unique properties, nanowires are widely used in modern technologies. For example, ferromagnetic nanowires (FNs) [1] are already considered as promising materials for targeted delivery of drugs, treatment of oncological diseases, warming up cryopreserved organs and biological tissues [2–6]. The application of FNs in data storage devices and nanosensors is also promising [7–9]. The idea of creating neural networks based on arrays of thin nanowires (≈1 nm) with electrical conductivity [10] looks promising and interesting as well. More detailed information on the practical application of nanowires can be found in the monographs [11, 12].

Among the wide variety of FNs, we select cylindrical nanowires. In these objects, the formation of domain walls (DWs) is possible. The stable magnetic configurations of these walls correspond to DWs of transverse type (the magnetisation vector $\vec{M}$ between neighbouring domains rotates perpendicularly to the DW plane), and DWs with the Bloch point. In this case, the thermal motion of DW is a significant factor affecting the thermodynamic and magnetocaloric properties of the cylindrical FNs (see Refs. [13–17]). In addition to the above types of DWs, an intermediate metastable state of the magnetisation vector distribution can form in the cylindrical FNs, so-called asymmetric DW [18]. In this connection, the papers [19–21] should be especially mentioned, where the conditions under which structural transitions between different types of DWs (transverse, asymmetric and DW with a Bloch point) in FNs take place are determined.

Many aspects related to the topological, structural and dynamic properties of BPs in DWs of various ferromagnetic nanosystems, such as magnetic bubble materials, nanowires, nanospheres and nanotubes, skyrmions, nanodisks and nanostrips, were studied theoretically and experimentally (see Refs. [22–41]). From the results of these investigations, it follows that when external fields are not applied, BP is in a metastable energy state and is localised in the centre of DW. At the same time, the demagnetising field of the ferromagnet can remove the degeneration of the magnetic structure of the DW sections separated by the BP, which leads to BP small oscillations. This case was considered in article [42] for BP in the DW of a cylindrical FN. In this work, the estimations for the maximum values of the natural frequency of BP oscillations in iron and nickel nanowires have been obtained. In addition, the possibility of practical implementation of the resonant oscillations of BP by an external alternating magnetic field was shown.

It should be noted that BP, along with other nanoscale magnetic topological solitons such as DW and vertical Bloch lines (subdomains inside DW), has quantum properties that in magnetic bubble materials have been investigated in works [43–52]. Quantum fluctuations of the magnetisation vector near the singularity centre of the Bloch point are considered in the article [53]. Thus, it is timely to study the quantum harmonic oscillations of BP in the domain wall of cylindrical FN. This problem in the quasi-classical approximation was considered in the paper [54]. The conditions for BP oscillations excitation in an external uniform magnetic field are established as well.

The above shows that the Bloch point in DW of cylindrical FN can be regarded as a harmonic oscillator. The grounding of this narrative based on works [21, 42, 50, 54] will be given in the present paper. In the first section of the paper, let us determine the magnetic structure of BP in the domain wall of cylindrical FN. The effective mass of BP will be specified in the second section. Further, using these results, we will study oscillatory properties of BP: classical and quantum. We will also consider the time evolution of the BP wave packet and determine the characteristic time of its transformation into beats and back.

2. Bloch Point Magnetic Structure

Let us find out the behaviour of the magnetisation vector $\vec{M}$ of the Bloch point. For this purpose, we write the expression for the density of the DW exchange energy w_e:

$$w_{\text{e}} = AM^{-2}\left(\left(\frac{\partial\vec{M}}{\partial x}\right)^2 + \left(\frac{\partial\vec{M}}{\partial y}\right)^2 + \left(\frac{\partial\vec{M}}{\partial z}\right)^2\right), \tag{1}$$

where A is the exchange constant.

Later, following Ref. [22], we find variation of expression $w_{\text{e}} - \lambda M^2$ with respect to vector $\vec{M}$, where λ is the indefinite Lagrange multiplier. Then, taking into account Eq. (1), we have for the $M_r = MR_r(r)\Phi_r(\varphi)Z_r(z)$ component of the magnetisation vector in a cylindrical coordinate system with the Oz axis directed along the longitudinal axis of the cylinder:

$$\frac{1}{\rho}\frac{\partial}{\partial\rho}\left(\rho\frac{\partial R_r}{\partial\rho}\right) + \left(\lambda - \lambda_1 - \frac{\lambda_2}{\rho^2}\right)R_r = 0, \tag{2}$$

where $\rho = r/\delta$, $z' = z/\delta$, $\delta = (A/M)^{1/2}$ —BP characteristic scale, λ_1 and λ_2 are the multipliers from the following equations: $d^2Z_r/dz'^2 + \lambda_1 Z_r = 0$, and $d^2\Phi_r/d\varphi^2 + \lambda_2\Phi_r = 0$. Similar relationships can be written for the components M_φ and M_z.

We seek solutions that are homogeneous in and near the centre of the Bloch point singularity: $z' \ll 1$, $\rho \ll 1$. This means that $\lambda_2 = 0$. Solution (2) provides the first order of smallness in z'. This solution corresponds to the first term in the expansion of the function $Z_r = \sin z'$ (we choose the constant equal to 1); so, $\lambda_1 = 1$. As a result, we obtain from Eq. (2) the zerothorder Bessel equation. Its solutions are the Bessel $J_0(\sqrt{\lambda-1}\rho)$ and Neumann $N_0(\sqrt{\lambda-1}\rho)$ functions. The latter has a logarithmic divergence at $\rho \to 0$. Choosing $N_0(\sqrt{\lambda-1}\rho)$ as a solution, and expanding it in a series at $\rho \ll 1$, we find

$$M_r = \frac{2}{\pi} M \left(\ln\left(\sqrt{\lambda-1}\rho\right) - 0.11593\right) z' . \quad (3)$$

Similarly, we also find the components M_z and M_φ of the magnetisation vector:b

$$M_z = \pm M\left(1 - z'^2/2\right), \ M_\varphi = 0 . \quad (4)$$

It is easy to verify that, taking the limit (ρ, z') to 0 at the singularity point, we get $M_r \to 0$ and $M_z \to \pm M$, as it should be. This proves the correctness of our solutions.

The factor λ is determined from the condition $M_r = Mz'$. We have also $M_r^2 + M_\varphi^2 + M_z^2 = 1$. So, using (3), we find $\lambda = 1 + 29.2/\rho^2$.

Taking into account this result and expressions (4), we write the formulas for the components of the vector $\vec{M}$ of the Bloch point in the small neighbourhood of the centre of the BP singularity in the final form:

$$M_r = M\, z/\delta, \quad M_\varphi = 0, \ \ M_z = \pm M(1 - z^2/2\delta^2). \quad (5)$$

It should be noted that solutions (5) correspond to the so-called 'divergent' magnetic structure of the Bloch point (Figs. 1, left and 2).

Besides BP magnetisation distribution (5), there can also be a convergent structure: $M_r = -M\, z/\delta$ $(\lambda = 1 + 0.054/(r/\delta)^2)$ (Fig. 1, right). The possibility of other magnetic configurations of BP, that are the result of unitary transformations of the coordinate axes, is considered in the papers [22, 25].

Later, from (5), we find that the magnetisation component M_z is equal to $-0.84M$ at $z = \delta_{\rm DW}$. In turn, the $\delta_{\rm DW} = \delta/\sqrt{\pi}$ is a parameter of the width of a transverse DW in which the distribution of the vector $\vec{M}$ along the OZ axis has the form $M_z = -M\tanh(z/\delta_{\rm DW})$ [13]. From this formula, we find that $M_z = -0.76M$ at the point $z = \delta_{\rm DW}$. Comparison of the above results shows that the $\delta_{\rm DW}$ can also be considered as a parameter of the DW width with the Bloch point.

Let us define the BP core as a region near the singularity centre in which $A/r_{\rm BP_c}^2$ — the exchange energy of BP by order of magnitude corresponds to $w_{m_n} \propto \pi M^2$ — the FN magnetostatic energy, which 'directs' the magnetisation vector along the OZ axis. In this case, the characteristic radius of the BP core is $r_{\rm BP_c} \propto \delta/\sqrt{\pi}$. It is easy to see that r_{BP_C} coincides with the expression for $\delta_{\rm DW}$.

The magnetic structure of BP, located before its core, can be considered as the transition region of BP. Obviously, its characteristic size is $\delta - \delta_{\rm DW}$. In the BP transition region, the deformation of the magnetic structure of the DW starts, which is a consequence of the effect of the

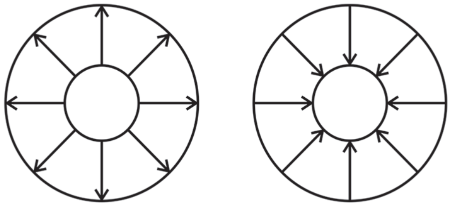

Fig. 1. Configurations of magnetisation vector in the small neighbourhood of the centre of BP singularity in cylindrical FN: left — magnetic structure directed from BP centre; right — magnetic structure directed to BP centre. The *OZ* axis of the cylindrical coordinate system is perpendicular to the page [21]

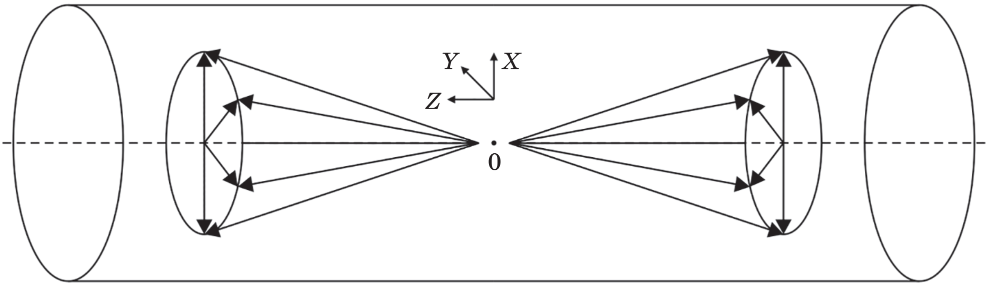

Fig. 2. Behaviour of the magnetisation vector near the singularity centre of a 'divergent' BP [42]

exchange field H_e on the field $H_{\vec{M}_\varepsilon}$ induced by the magnetic moment $\vec{M}_\varepsilon = 4\pi\vec{M}r_\varepsilon^3/3$ in an infinitesimally small neighbourhood of radius r_ε. In this region, the interaction of $\vec{M}_\varepsilon$ with other magnetic moments of the ferromagnet is not taken into account (see in Ref. [55]). In this case, the magnetic field of the remaining part of the dipole sum ($r > r_\varepsilon$) exceeds the field H_e. Obviously, the vector $\vec{H}_e$ is oriented in the same direction as the 'magnetic anisotropy' field, *i.e.*, either along or opposite the normal to the DW. As a result, the magnetisation vector deviates from its direction in the central plane of the DW. Since $H_e \approx \langle H_{\vec{M}_\varepsilon} \rangle$ (where $\langle H_{\vec{M}_\varepsilon} \rangle = 2M$ is the magnitude of $H_{\vec{M}_\varepsilon}$ averaged over the directions of the normal to the DW) in the transition zone, it is natural to assume that this effect is small in this DW zone; however, it sharply increases ($H_e \gg \langle H_{\vec{M}_\varepsilon} \rangle$) in the centre of the core. At this point, the magnetisation is directed strictly along the normal to the central section of the DW plane.

The radius of the vortex magnetic structure decreases with further approach to the core. The minimum value of the radius at which this distribution of the magnetisation vectors still takes place is determined by the core scale. The structure itself appears in the form of two pairs of oppositely oriented magnetisation vectors $\vec{m}$ directed along the tangents to the circle of radius δ_{DW} (Fig. 3). This is the minimum magnitude of $\vec{m}$ needed for vortex forming. In this case, the absolute values of $\vec{m}$ (as well as the area of the cell formed by them) are the lowest magnetisation vectors in the central plane of the DW. It is easy to see that the development of the vortex structure according to the directions (displacement and rota-

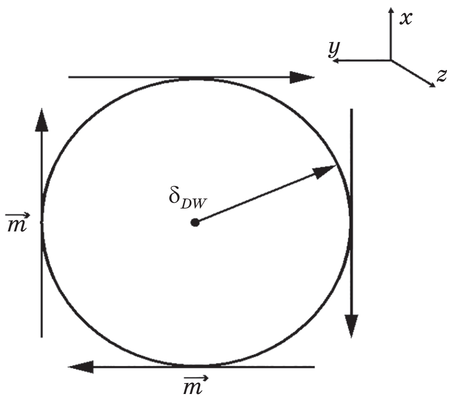

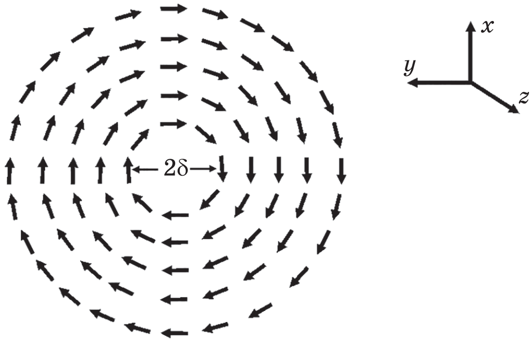

Fig. 3. Primitive vortex cell of DW with the Bloch point. The vectors $\vec{m}$ determine both the spatial development of the magnetic structure of a DW with the Bloch point and the direction of rotation of the magnetisation vectors in it. The *OX* and *OY* axes of the Cartesian coordinate system are oriented along the vectors $\vec{m}$ [42]

Fig. 4. Distribution of magnetisation vectors $\vec{M}$ in the central plane of DW with the Bloch point [42]

tion) determined by the vectors $\vec{m}$ leads to the formation of a DW with a Bloch point (Fig. 4).

Considering the above, it is natural to name this magnetic configuration 'a primitive vortex cell', by analogy with the crystallographic term. Similarly, a cell is also confirmed by the result obtained by means of micromagnetic simulation of the magnetic structure of a DW with a Bloch point in a cylindrical permalloy nanowire in Ref. [19]. Further analysis will be carried out in a rectangular Cartesian co-ordinate system with *OX* and *OY* axes oriented along the spatial directions of the vector $\vec{m}$. We will also neglect the normal component of the vector $\vec{M}$ in the transition zone of the Bloch point. This means that the magnetic structure of this section of the DW has a vortex nature solely.

Note that, using the concept of 'a primitive vortex cell', in the article [56], a fractal algorithm of structure building of the magnetic structure of the central plane of the DW with a Bloch point was proposed.

3. Bloch Point Effective Mass

Let us consider the displacement of the BP. Since the magnetic structure of the DW should be preserved in this case, the motion of the BP occurs along the spatial directions of the primitive vortex cell. Taking into account this fact, and assuming the process to be self-stimulating, we consider the displacement of the soliton along the *OX* axis of the Cartesian coordinate system. In this case, the velocity of the Bloch point centre $\dot{x}_{\mathrm{BP}}$ should be significantly lower than the velocity of the precession of vector

$\vec{M}_y$ around the demagnetisation field of the Bloch point $\vec{H}'_{d_y} \approx -4\pi\vec{M}_y$. This field has the maximum value $\approx -4\pi M$ at the point $x = 0$, $y = \delta$, and is equal to zero at the centre of BP. The actual scale corresponding to the characteristic change of this field is δ. Taking the average value $H'_{d_y} \approx -2\pi M$ in this interval, we get

$$\dot{x}_{\rm BP} \ll 2\pi M\gamma\delta, \tag{6}$$

where $\gamma = 2\cdot 10^7$ Oe/s is the gyromagnetic ratio.

The effective mass of the Bloch point $m_{\rm BP}$ is found from the relation [57]

$$\frac{1}{2}F_z q_{{\rm BP}_z} = \frac{1}{2}m_{\rm BP}\dot{x}^2_{\rm BP}, \tag{7}$$

where $F_z = \int dxdydz f_{g_z}$ is the force that initiates the local bending of the domain wall centre $q_{{\rm BP}_z}$ whose sign is determined by the gyrotropic Thiel force $\vec{f}_{g_z} = (M/\gamma)\left[\vec{g}_y \times \dot{\vec{x}}_{\rm BP}\right]$, $\vec{g}_y = -\sin\theta\left[\vec{\nabla}_z\theta \times \vec{\nabla}_x\varphi\right]$ is the gyrotropic vector, θ and φ are the polar and azimuth angles of the vector $\vec{M}$, respectively [58].

Given the explicit form of $\vec{f}_{g_z}$, the force F_z can be written as

$$F_z = -\frac{M}{\gamma}\dot{x}_{\rm BP}\int dz\frac{\partial}{\partial z}\cos\theta\int dxdy\frac{\partial\varphi}{\partial x}. \tag{8}$$

The finite value of $q_{{\rm BP}_z}$ indicates the movement of the Bloch point with a speed $\dot{x}_{\rm BP}$ along the OZ axis. The self-stimulating condition in this case is obviously equivalent to the inequality

$$q_{{\rm BP}_z} \ll \delta_{\rm DW}. \tag{9}$$

Since (6) and (9) characterise the same self-stimulating process, it is natural to assume that the ratio $\dot{x}_{\rm BP}/2\pi\gamma M\delta$ has the same order of smallness as the term $q_{{\rm BP}_z}/\delta_{\rm DW}$: $\dot{x}_{\rm BP}/2\pi\gamma M\delta \cong q_{{\rm BP}_z}/\delta_{\rm DW}$.

Using this formula, we find $q_{{\rm BP}_z}$, and after integration in Eq. (8), we obtain the expression for the effective mass of the Bloch point in its transition zone from (7):

$$m_{\rm BP} = \frac{2\delta_{\rm DW}}{\gamma^2}\left(1 - \frac{\delta_{\rm DW}}{\delta}\right). \tag{10}$$

Let us now consider the core zone. In this case, the characteristic zone of spin wave propagation is limited by the scale $\delta_{\rm DW}$. Then $q_{{\rm BP}_z}$ is determined from the relation $\dot{x}_{\rm BP}/2\pi\gamma M\delta_{\rm DW} \cong q_{{\rm BP}_z}/\delta_{\rm DW}$: $q_{{\rm BP}_z} = \dot{x}_{\rm BP}/2\pi\gamma M$.

Taking into account this result, formulas (5), from which it follows that $\int_{-\delta_{\rm DW}}^{\delta_{\rm DW}} dz\frac{\partial}{\partial z}\cos\theta = 2\int_0^{\delta_{\rm DW}} dz\frac{\partial}{\partial z}\cos\theta = (\delta_{\rm DW}/\delta)^2$, and the fact that $\varphi|_{x=\delta_{\rm DW}} - \varphi|_{x=-\delta_{\rm DW}} = \pi$ (see also Fig. 3), Eqs. (8) and (7), we obtain the expression for the effective mass of the Bloch point in the zone of its core:

$$m_{\rm BP} = \frac{\delta_{\rm DW}}{\gamma^2}(\delta_{\rm DW}/\delta)^2. \tag{11}$$

An analysis of formulas (10) and (11) shows that the order of magnitude of the effective mass of a point soliton is determined by the magnetic structure of the zone transitional to its core:

$$m_{\mathrm{BP}} \cong \delta_{\mathrm{DW}} / \gamma^2. \tag{12}$$

The same expression was obtained for the effective mass of the BP in a ferromagnet with strong uniaxial magnetic anisotropy [59]. The coincidence of these formulas is a consequence of the uniaxial nature of the magnetic anisotropy of the systems. In both cases, the main contribution to the effective mass comes from the magnetic structure of the BP transition zone. Obviously, Eqs. (10)–(12) are also applicable when the BP moves along the OY axis due to the symmetry of the system under consideration. For iron and nickel cylindrical nanowires, we obtain the following results from Eq. (12): $m_{\mathrm{BP_{Fe}}} \approx 1.2 \cdot 10^{-21}$ g and $m_{\mathrm{BP_{Ni}}} \approx 2.8 \cdot 10^{-21}$ g.

4. Bloch Point Harmonic Oscillations

Let us now consider the possibility of harmonic oscillations of BP in a cylindrical FN. For this process, the soliton should be affected by a force directed against the movement and depending on the displacement coordinate, in addition to having an inertial characteristic (mass). The source of such a force is the demagnetisation field of the FN, which ‘directs’ the magnetisation vectors of a transverse DW along the tangents to the concentric circles in the central section of the DW. To find this field, we will assume that the nanowire radius a significantly exceeds δ_{DW}. Let us consider the semicircles along which the magnetic charges, induced by the component M_x of the magnetisation vector of the transverse DW in the near-surface layer of the FN, are located. The layer thickness is assumed equal to δ_{DW}. The choice of δ_{DW} as a measure of smallness, and, accordingly, proximity to the surface of the nanowire, is explained by the minimum value of this scale among the characteristic dimensions of the systems under consideration.

Taking into account this approximation, the semicircles can be considered as thin ‘threads’ perpendicular to the corresponding directions of their radii. Based on [60], we can write the following expression for the magnetic field scalar potential ψ [61] in the layer δ_{DW}, induced by the ‘threads’ oriented along the OY axis:

$$\psi = 2\tau_1 \ln \delta_{\mathrm{DW}} + 2\tau_2 \ln 2a, \tag{13}$$

where $\tau_{1,2} = dq_{m_{1,2}} / dl$ is the density of magnetic charges per unit length of the ‘thread’ of the upper and lower semicircles of the DW, respectively, $dq_{m_{1,2}}$ is the magnetic charge of an infinitely small section dl of the ‘thread’.

In turn, the density of the surface magnetic charges $\sigma_{1,2}$ is

$$\sigma_{1,2} = \partial^2 q_{m_{1,2}} / \partial l \partial l', \tag{14}$$

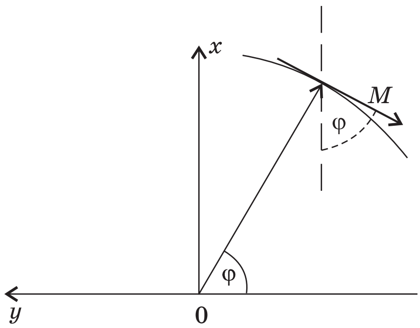

Fig. 5. Fragment of vortex magnetic structure of the transition zone of the Bloch point; $\mathrm{tg}\varphi = x/y$, $y < 0$. The angle between the vector M and the OX axis is $\pi - \varphi$ [42]

where dl' is the infinitesimally small width element of the 'thread'. Since $dl' = dl$ and $\sigma_{1,2} = \pm M$ for a thin 'thread' (in the case under consideration), it is easy to find from Eq. (14) by integrating over dl that $\tau_1 = -\tau_2 = \pm\pi a M$.

Next, multiplying the magnetic potential ψ by $\rho_m/2$, where $\rho_m \cong \cong \Delta\sigma/\pi a = 2M/\pi a$ is the volume density of magnetic charges, and taking into account Eq. (13), we obtain an expression $w_{\delta_{\mathrm{DW}}} = \pm 2M^2 \ln 2a/\delta_{\mathrm{DW}}$ for the specific demagnetisation energy in a thin layer δ_{DW}.

From this relation, we determine the magnetic field $H_{\delta_{\mathrm{DW}_y}}$:

$$H_{\delta_{\mathrm{DW}_y}} = \mp 4M \ln 2a/\delta_{\mathrm{DW}}. \tag{15}$$

Obviously, the value of the demagnetisation field should decrease with approaching to the centre of the DW, and it becomes zero at the point $x = 0$. Taking into account this fact, and basing on Eq. (15), we can write the following model expression for the demagnetisation field H_{d_y} that acts on the magnetic structure of a DW with the Bloch point:

$$H_{d_y}(x) = \mp 4M \ln \frac{a + x}{a - x}. \tag{16}$$

It is worthwhile to note that expression (16) is similar to the formula for the demagnetisation field induced by the surface magnetic charges of a Bloch DW inside a uniaxial ferromagnetic film [62].

Assuming the variable x is the coordinate of the displacement of the Bloch point centre x_{BP} in the expression (16), we can write the interaction energy of the Bloch point $W_{\mathrm{BP},H_{d_y}}$ with the field $\vec{H}_{d_y}$ after a series of transformations as

$$W_{\mathrm{BP},H_{d_y}} = \frac{8M^2}{a} x_{\mathrm{BP}} \int dx dy dz \sin\theta \sin\varphi. \tag{17}$$

Let us expand it in the series $\sin\varphi \cong \sin\varphi_0 + \cos\varphi_0 x_{\mathrm{BP}} \dfrac{\partial\varphi_0}{\partial x}$, where $\mathrm{tg}\varphi_0 = = x/y$ is the vortex solution for the distribution of the magnetisation vector (see Fig. 5); we also take into account that in the DW zone the relation $\sin\theta \simeq \delta_{\mathrm{DW}}\, \partial\theta/\partial z$ takes place. We find from Eq. (17) after integrating over the transition zone of the Bloch point: $W_{\mathrm{BP},H_{d_y}} = \dfrac{1}{2} 16M^2\pi^2\delta_{\mathrm{DW}} \left(\dfrac{\delta - \delta_{\mathrm{DW}}}{a}\right) x_{\mathrm{BP}}^2$.

According to Eq. (5), the contribution of the Bloch point core zone to the energy of interaction with the field H_{d_y} can be assumed equal to zero.

The above expression allows us to find the stiffness coefficient $k_{\mathrm{BP}} = 16\pi^2 M^2 \delta_{\mathrm{DW}}(\delta - \delta_{\mathrm{DW}})/a$. Using Eq. (10), we obtain the formula for the natural frequency of the Bloch point harmonic oscillations $\omega_{\mathrm{BP}} = \sqrt{k_{\mathrm{BP}}/m_{\mathrm{BP}}}$:

$$\omega_{\mathrm{BP}} = \left(\frac{\delta}{2a}\right)^{1/2} \omega_M, \tag{18}$$

where $\omega_M = 4\pi\gamma M$.

It should be noted that the value of ω_{BP} in formula (18) differs from the similar parameter of the Bloch point in Ref. [56] by a coefficient $1/\sqrt{2}$. This is a consequence of large Q values (the quality factor of magnetic films that was considered in Ref. [59]). In our case, we have $Q = \pi$ (see in Ref. [21]). Therefore, formula (18) coincides with the expression for the frequency of natural vibrations of the Bloch point in Ref. [59] only in the order of magnitude. The same holds for formula (8) for the effective mass of a Bloch point.

Taking into account the criterion for the formation of a DW with a Bloch point in a nanowire $\ln a/\delta \geq \pi$ [21], we find from Eq. (18) $\omega_{\mathrm{BP}} \leq e^{-\pi/2}\omega_M/\sqrt{2}$. Using this relation, we determine the maximum values of the natural frequencies of the Bloch point in iron and nickel nanowires: $\omega_{\mathrm{BP}_{\mathrm{Fe}}} \approx 10$ GHz and $\omega_{\mathrm{BP}_{\mathrm{Ni}}} \approx 3$ GHz, respectively.

Note that expression (18) corresponds to the frequency of harmonic oscillations of a Bloch point relative to the *OX* and *OY* axes of the chosen coordinate system. Therefore, to excite the resonant oscillations of the Bloch point, it is necessary to have an external alternating magnetic field applied along one of the indicated directions. This field removes the energy degeneracy of the DW segments separated by the Bloch point along another axis. As a result, the Bloch point moves, and the elastic force from the demagnetisation field counteracts that.

It should be said that the effect of demagnetisation fields H_{d_x} and H_{d_y} on the Bloch point magnetic structure leads to the occurrence of torsional oscillations of the Bloch point about the axis *OZ* as well. Setting in formula (16) $x = a - \delta$, and assuming the moment of inertia of the Bloch point to be $m_{\mathrm{BP}}\delta^2/2$, after a series of simple transformations, we find the small oscillations frequency $\frac{\omega_M}{\sqrt{\pi}}\sqrt{\ln 2a/\delta} \geq \sqrt{\frac{\ln 2 + \pi}{\pi}}\omega_M \approx \omega_M$. The rotational properties of the primitive vortex cell cause this result.

Let us consider oscillations of the Bloch point along the *OX* axis under the action of an external magnetic field $\vec{H}_y = H_0 \cos\Omega t \vec{e}_y$. Integrating the interaction energy of this field with the Bloch point and taking into account Eq. (10), it is easy to obtain the following equation for the Bloch point oscillations:

$$\ddot{x}_{\mathrm{BP}} + 2\alpha_r' \omega_M x_{\mathrm{BP}} + \omega_{\mathrm{BP}}^2 x_{\mathrm{BP}} = \frac{1}{4}\omega_M^2 \delta h_0 \cos\Omega t, \tag{19}$$

where $\alpha'_r = \dfrac{\alpha_r\sqrt{\pi}}{8(\sqrt{\pi}-1)}(\pi + 0.5\ln\pi)$, α_r is the damping ratio of the magnetisation vector, and $h_0 = H_0/8M$.

In Eq. (19), the term corresponding to the dissipation of the magnetisation vector was determined by integrating the dissipative function over the region of the BP. Based on Ref. [63], the density of the dissipative function can be written as follows: $\vec{f}_r = -\alpha_r \dfrac{M}{\gamma}\Big[(\partial\theta/\partial z)^2 + \sin^2\theta\left(\partial\varphi_0/\partial x\right)^2\Big]\dot{x}_{\mathrm{BP}}\vec{e}_x$.

Integrating this expression over the core region, we assumed $(\partial\theta/\partial z)^2 \approx \delta_{\mathrm{DW}}^{-2}\cos^2\theta$. Taking into account the term $\propto \sin^2\theta$ in this segment takes us beyond the approximation in which the formulas (5) were obtained.

Using Eq. (18), from Eq. (19), we find the frequency Ω_{r} of the Bloch point resonant oscillations and corresponding amplitude $x_{\mathrm{BP_r}}$:

$$\Omega_{\mathrm{r}} = \omega_M\sqrt{\frac{\delta}{2a} - 2\left(\alpha'_r\right)^2}, \quad x_{\mathrm{BP_r}} = \frac{\delta h_0}{8\alpha'_r\sqrt{\dfrac{\delta}{2a} - \left(\alpha'_r\right)^2}}. \tag{20}$$

It is natural to assume that the oscillation amplitude $x_{\mathrm{BP_r}}$ does not exceed the characteristic size of the system δ. Then, assuming $\delta/a \cong e^{-\pi}$ and $\alpha_r \cong 10^{-3}$ (we consider the case of low attenuation), we obtain the estimate for the magnitude of the amplitude of the external magnetic field from (20): $h_0 \le 10^{-3}$. In this case, the resonant frequency is $\Omega_{\mathrm{r}} \approx \omega_{\mathrm{BP}}$.

An analysis of the next non-zero term in the expansion of the energy of interaction of the Bloch point with the field $\vec{H}_y$ shows that it is lower by a factor of $\simeq (x_{\mathrm{BP}}/\delta)^2$ than the linear term in Eq. (19). Obviously, an equation similar to Eq. (19) can also be obtained for an alternating magnetic field oriented along the *OX* axis. In this case, the forced oscillations of the Bloch point occur along the *OY* axis of the Cartesian coordinate system.

Let us consider the possibility of implementing resonant oscillations of the Bloch point, estimating the quality factor of the system $\tilde{Q}$. To do this, we use formula $\tilde{Q} = \omega_{\mathrm{BP}}/\Delta\omega_{\mathrm{r}}$, where $\Delta\omega_{\mathrm{r}}$ is the width of the resonance curve. In the case of weak attenuation, we have $\Delta\omega_{\mathrm{r}} = 2\sqrt{3}\alpha'_r\omega_M$ [64]. Taking into account the explicit form of the coefficient α'_r (see Eq. (19)), and assuming $\alpha_r \cong 10^{-3}$, $\delta/a \cong 5\cdot 10^{-2}$, we find $\tilde{Q} \approx 43$. This value of the quality factor exceeds 30, which indicates the possibility of experimental observation of the resonant harmonic oscillations of the BP by means of radio frequency measurements.

5. Bloch Point Quantum Oscillations

Based on the general principles of the theory of a quantum oscillator [65], we can write the energy of the BP quantum oscillations E_{BP_n} as

$$E_{\mathrm{BP}_n} = \hbar\omega_{\mathrm{BP}} n, \tag{21}$$

where $\hbar$ is the Planck constant, $n \gg 1$ is the principal quantum number. The BP oscillations occur along the basis vectors of the primitive vortex cell (in our case, along the OX or OY axes).

Within the quasi-classical approximation, the amplitude of harmonic oscillations A_{BP_n} is determined by comparing its total oscillation energy $m_{\mathrm{BP}}\omega_{\mathrm{BP}}^2 A_{\mathrm{BP}_n}^2/2$ and energy (21):

$$A_{\mathrm{BP}_n} = \sqrt{\frac{2\hbar n}{m_{\mathrm{BP}}\omega_{\mathrm{BP}}}}. \tag{22}$$

Suppose that oscillations of the BP occur along the OX axis. Then quantum transitions to the quasi-classical region of the BP energy spectrum can be induced by an external uniform magnetic field $\vec{H}_x = H\vec{e}_x$ (where $\vec{e}_x$ is the unit vector along the OX axis). In this case, according to Ref. [50], the average energy $W_{\mathrm{BP},\vec{H}_x}/2$ of the BP interaction with the field $\vec{H}_x$ should significantly exceed the interlevel energy $\hbar\omega_{\mathrm{BP}}$. Using Eq. (19), we can write

$$\frac{1}{2}W_{\mathrm{BP},\vec{H}_x} = -\frac{1}{8}\omega_M^2 \delta h m_{\mathrm{BP}} \langle x_{\mathrm{BP}} \rangle, \tag{23}$$

where $h = H/8M$, and $\langle x_{\mathrm{BP}} \rangle$ is the average displacement of the BP centre under the influence of the magnetic field.

Equating $\frac{1}{2}W_{\mathrm{BP},\vec{H}_x}$ to $-\frac{1}{2}m_{\mathrm{BP}}\omega_{\mathrm{BP}}^2 \overline{x}_{\mathrm{BP}}^2$, we determine the average displacement $\langle x_{\mathrm{BP}} \rangle = \omega_M^2 h\delta/4\omega_{\mathrm{BP}}^2$. After substituting this expression into Eq. (23) and taking into account the relation $W_{\mathrm{BP},H_x}/2 \gg \hbar\omega_{\mathrm{BP}}$, we find the amplitudes of the magnetic fields that provide the quasi-classical nature of the oscillation process:

$$h \gg h_q = \frac{2}{\pi}\left(\frac{\delta}{2a}\right)^{3/4} \sqrt{\hbar\omega_M/E_{\mathrm{BP}_c}}, \tag{24}$$

where $E_{\mathrm{BP}_c} = 2A\delta/\sqrt{\pi}$ is the energy of the BP core [21].

Let us now derive an expression for evaluating the magnitudes of magnetic fields for which we can neglect the force of viscous damping of magnetisation, F_r.

Referring to formula (19), we can write the force F_r as

$$F_r = 2\alpha_r'\omega_M\omega_{\mathrm{BP}} A_{\mathrm{BP}_n} m_{\mathrm{BP}}. \tag{25}$$

Then, according to Eqs. (22), (23), and (25), the force F_r can be neglected for magnetic field amplitudes

$$h \gg h_r = \frac{4\alpha_r'}{\pi}\left(\frac{\delta}{2a}\right)^{1/4} \sqrt{\frac{\hbar\omega_M}{\sqrt{\pi}E_{\mathrm{BP}_c}}}. \tag{26}$$

Note that the quantum nature of the BP motion should also manifest itself in the corresponding behaviour of the DW gyrotropic bending caused by the BP dynamics. Actually, taking into account formula (23) and the expression for the DW gyrotropic bending in the core zone (see above), we find that the 'quantisation' q_{BP_n} bending also occurs:

$$q_{\mathrm{BP}_n} \cong \frac{\omega_{\mathrm{BP}} A_{\mathrm{BP}_n}}{2M\gamma} = \left(\frac{\delta}{2a}\right)^{1/4} \sqrt{\frac{\hbar\omega_M n}{E_{\mathrm{BP_c}}}}\,\delta\,. \tag{27}$$

Let us evaluate the formulas (27) for nickel and iron nanowires with the following parameters: $A_{\mathrm{Ni}} \cong 10^{-6}$ Oe/cm, $A_{\mathrm{Fe}} \cong 2\cdot 10^{-6}$ Oe/cm, $M_{\mathrm{Ni}} \cong$ $\cong 5\cdot 10^2$ Gs, $M_{\mathrm{Fe}} \cong 1.7\cdot 10^3$ Gs, $n \cong 10$. In this case, we take into account that, according to Ref. [21], the radius of the nanowire, in which the BP forms, satisfies the relationship $(\delta/a) \le e^{-\pi}$. Then, we find from Eqs. (24), (26), and (27): $h_{q_{\mathrm{Ni}}} \cong 2.5\cdot 10^{-4}$, $h_{r_{\mathrm{Ni}}} \cong 10^{-4}$–$10^{-5}$ and $h_{q_{\mathrm{Fe}}} \cong 5.4\cdot 10^{-4}$, $h_{r_{\mathrm{Fe}}} \cong$ $\cong 2\cdot(10^{-4}$–$10^{-5})$, $q_{\mathrm{BP}_{n_{\mathrm{Ni,Fe}}}} \ge 10^{-2}\delta$.

It is easy to see that the obtained values of magnetic fields indicate the possibility of their practical application. Their smallness compared to $8M$ allows neglecting the effect of the fields on the DW magnetic structure [22]. Besides, we have $h_{q_{\mathrm{Ni}}} \ge h_{r_{\mathrm{Ni}}}$ and $h_{q_{\mathrm{Fe}}} \ge h_{r_{\mathrm{Fe}}}$. In turn, the estimate for q_{BP_n} is consistent with the condition of locality of the DW gyrotropic bending: $q_{\mathrm{BP}_n} \ll \delta$.

It should be said that w_n as the probability of the distribution $\tilde{n} = W_{\mathrm{BP},H_x}/2$ of quanta over n discrete levels of a quantum oscillator is described by the Poisson distribution (see Ref. [65]): $w_n = \frac{1}{n!} e^{-\tilde{n}} \tilde{n}^n$.

Analysis of this expression shows that the maximum probability of realising quantum state $n \cong 10$ is achieved at $\tilde{n} \cong 10$. Taking into account this fact, it is easy to show that the amplitudes of the magnetic fields that provide excitation of a given energy level in nickel and iron nanowires are $h_{q_{\mathrm{Ni}}} \cong 2.5\cdot 10^{-3}$ and $h_{q_{\mathrm{Fe}}} \cong 5.4\cdot 10^{-3}$, respectively.

The temperature T_q at which quantum oscillations of BP can actually be estimated by the following formula

$$T_q = n\hbar\omega_{\mathrm{BP}}/k_B, \tag{28}$$

where k_B is the Boltzmann constant.

Considering that the maximum values for Ni and Fe nanowires are 3 and 10 GHz, respectively (see above), and assuming the principal quantum number $n \cong 10$, we find the following estimates from Eq. (28): $T_{q_{\mathrm{Ni}}} \le 1.4$ K and $T_{q_{\mathrm{Fe}}} \le 4.6$ K.

Thus, in these nanosystems, the temperatures at which quantum oscillations of BP occur correspond to the temperatures at which helium is liquid. Moreover, the obtained $T_{q_{\mathrm{Ni}}}$ and $T_{q_{\mathrm{Fe}}}$ values indicate the macroscopic nature of the process. Actually, given that the effective mass of a magnon is of $\approx 10^{-26}$ g [66], and we have $m_{\mathrm{BP_{Ni}}} \approx 2.8 \cdot 10^{-21}$ g and $m_{\mathrm{BP_{Fe}}} \approx 1.2 \cdot 10^{-15}$ g for BP in the nickel and iron nanowire, respectively (see above), it is not difficult to determine that the number of magnons participating in quantum oscillations is of $\cong 10^5$. This result allows us to classify this phenomenon as a magnetic macroscopic quantum effect.

It should be especially noted that formulas (19), (26) were obtained using the phenomenological description of magnetic relaxation in the Landau–Lifshitz equation for the magnetisation vector in a ferromagnet [67]. At the same time, taking into account the relaxation terms of the exchange nature in this equation [68] leads to a rather high magnetic aftereffect appearing during the BP movement [69], which was observed in an experiment in yttrium–iron garnet at room temperature [70]. Let us show that this effect can be neglected at lower temperatures.

Based on the Bloch's $T^{1/2}$ law for magnetisation, we can write the following expression (see Ref. [71]):

$$\frac{\Delta M}{M(0)} = \frac{0.0587}{SQ}\left(\frac{k_B T}{JS}\right)^{1/2}, \qquad (29)$$

where $\Delta M = M(0) - M(T)$ is the deviation of magnetisation from its magnitude $M(0) = M$ at $T = 0$ K, the parameter $Q = 2.4$ for b.c.c. and f.c.c. lattice, respectively, S is the average value of the spin number, and J is the exchange integral.

At the same time, we can write using the mean-field model [71]: $J = \dfrac{3k_B T_C}{2zS(S+1)}$, where z is the number of nearest neighbours, and T_C is the Curie point of a ferromagnet.

Substituting the above expression into formula (29), and also assuming $S \approx 1$, $z_{\mathrm{Ni}} = 12$, $z_{\mathrm{Fe}} = 8$, $T_{C_{\mathrm{Ni}}} = 631$ K, $T_{C_{\mathrm{Fe}}} = 1043$ K for the temperatures of liquid helium, we estimate $\Delta M/M \cong 10^{-3}$, which indicates the smallness of the effect of changing the magnitude of magnetisation due to the exchange interaction. This result allows us to ignore the corresponding relaxation terms in the Landau–Lifshitz equation.

6. Bloch Point Wave Packet Time Evolution

The quantum dynamics of BP in space can be described by a wave packet (WP) which is a superposition of $2m+1$ $(1 \ll m \ll n)$ eigenfunctions of the quantum oscillator in the quasi-classical approach [72]:

$$\varphi_n(\xi, t) = \frac{1}{\sqrt{2m+1}} \sum_{k=-m}^{m} \frac{1}{\sqrt{2^{n+k}\sqrt{\pi}x_0}} e^{-\frac{1}{2}\xi^2} H_{n+k}(\xi) e^{i\omega_{\mathrm{BP}}(n+m)t}, \qquad (30)$$

where $\xi = x/x_0$, $x_0 = \sqrt{\hbar/m_{\mathrm{BP}}\omega_{\mathrm{BP}}}$, t is the time, and $H_{n+k}(\xi)$ are the Hermite polynomials.

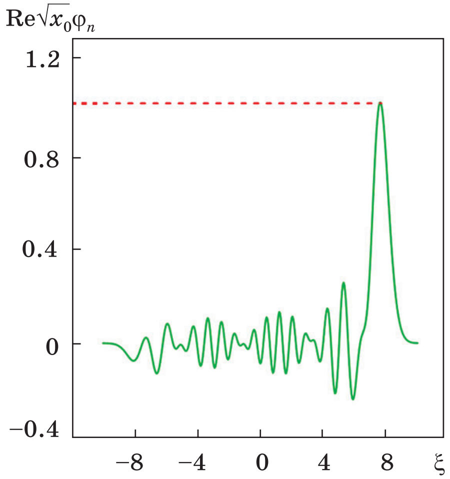

Fig. 6. Wave packet in the point $t = 0$ [54]

The function $\sqrt{x_0}\varphi_n$ at $n = 30$, $m = 5$, $t = 0$ is shown in Fig. 6. As expected, the centre of gravity of WP (position of the most probable location of BP) is localised near the wall ($\xi = (A_{\mathrm{BP}_n}/x_0)^{1/2} \approx 7.7$) of the potential well of the oscillator. Its co-ordinate is ≈7.6. At this point, $\mathrm{Re}\sqrt{x_0}\varphi_n = \sqrt{x_0}\varphi_n \approx 1$. Moreover, the equilibrium position of the oscillator shifts by $\langle x_{\mathrm{BP}}\rangle$ (see the derivation of formula (24)). We will consider the WP dynamics in relation to this point.

Let us find the time after which the WP smearing occurs. Since the characteristic scale of interaction of the potential with the quasiparticle is $\propto x_0$ (see wave functions in Eq. (30)), it is natural to take this distance as the effective width of the WP main maximum. Assuming that the shape of this profile is symmetrical, we conclude that the smearing of the packet occurs when its centre of gravity fluctuates by a critical value $\Delta x \propto x_0/2$. Then, the corresponding time, after which the transformation of the WP will occur, can be determined as $t_{\mathrm{tr}} = \Delta x \big/ 2\sqrt{\langle v^2\rangle}$, where $\langle v^2\rangle$ is the root-mean square velocity of the WP centre of gravity.

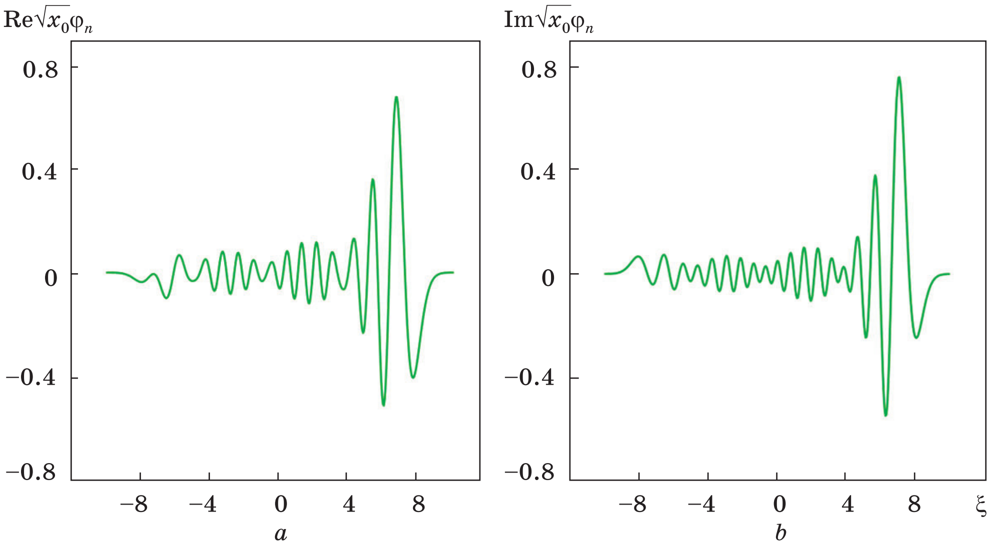

Fig. 7. Wave packet in the point $t = 0.5/\omega_{\mathrm{BP}}$: (*a*) the real part of WP; (*b*) the imaginary part of WP [54]

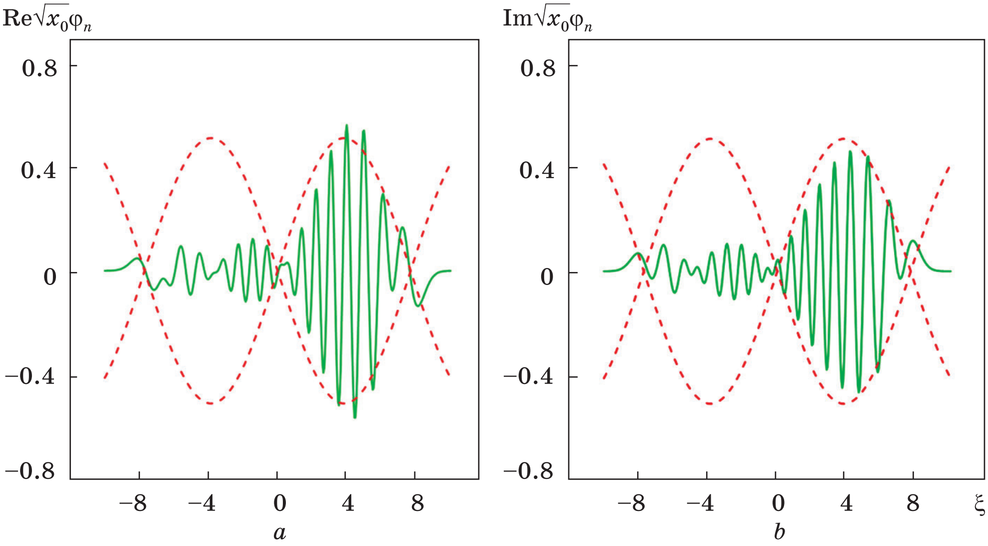

Fig. 8. The same as in the previous figure, but for $t = t_{\rm tr} \propto \omega_{BP}^{-1}$ [54] (dashed curves correspond to the function, which envelopes the beats)

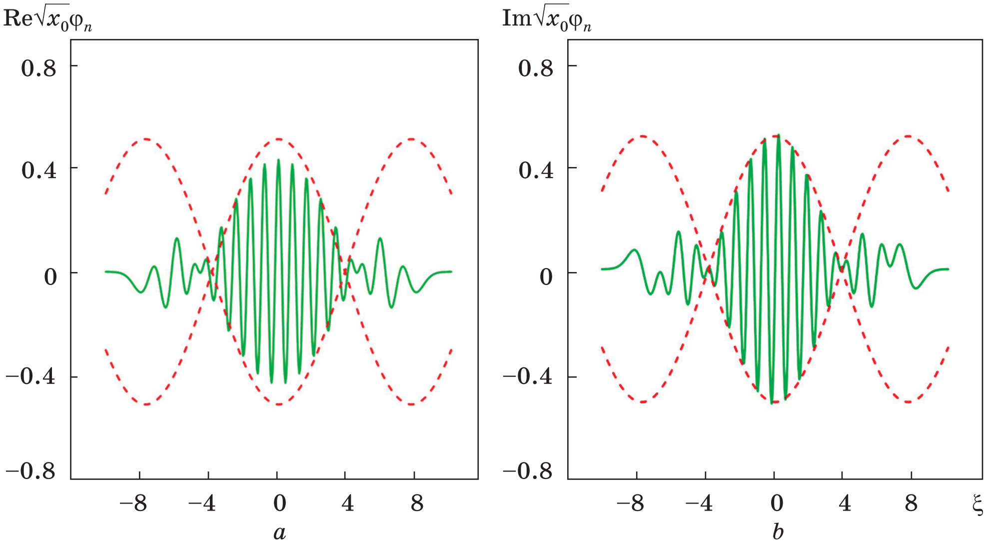

Fig. 9. The same as in the previous figure, but for $t = \pi/2\omega_{\rm BP}$ [54]

Using further the Heisenberg uncertainty principle, which in our case can be written as $m_{\rm BP}\sqrt{\langle v^2\rangle}\Delta x \geq \hbar/2$, it is easy to find from the above formula that $t_{\rm tr} \leq \omega_{\rm BP}^{-1}$.

Obviously, the above result does not depend on the specific material of the nanowire. However, it should be considered as an estimate due to the assumptions we made, and it should be accepted that $t_{\rm tr} \cong \omega_{\rm BP}^{-1}$.

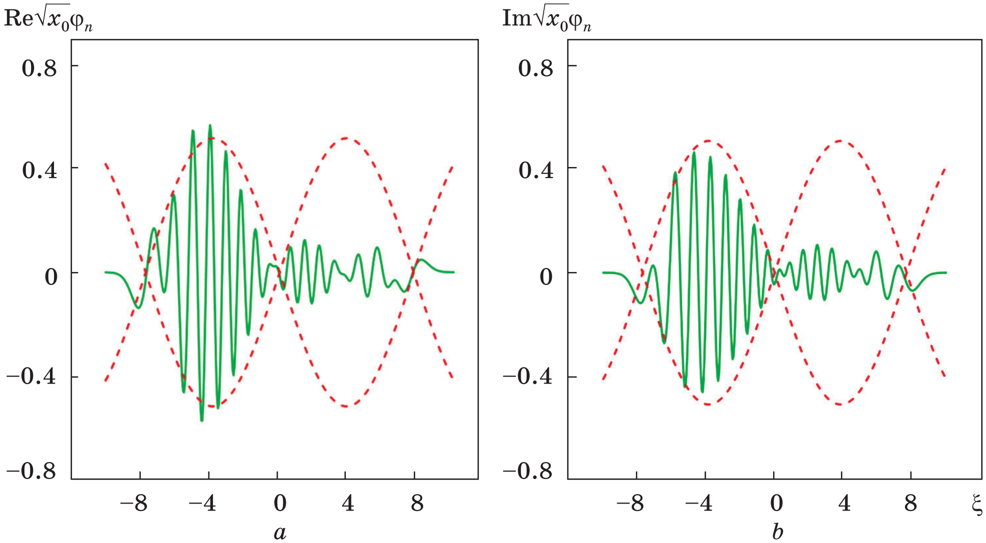

Fig. 10. The same as in the previous two figures, but for $t = \pi/\omega_{\mathrm{BP}} - t_{\mathrm{tr}}$ [54]

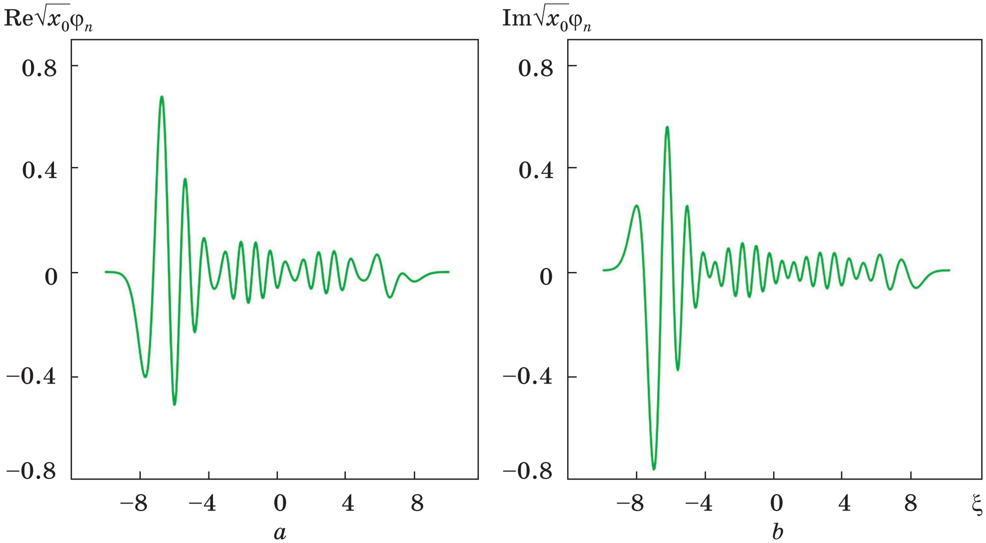

Fig. 11. The same as in Fig. 7, but for $t = (\pi - 0.5)/\omega_{\mathrm{BP}}$ [54]

Let us now consider the behaviour of the WP in the following points: $t = 0.5/\omega_{\mathrm{BP}}$ (Fig. 7), $t = t_{\mathrm{tr}} \cong \omega_{\mathrm{BP}}^{-1}$ (Fig. 8), $t = \pi/(2\omega_{\mathrm{BP}})$ (Fig. 9) and $t = \pi/\omega_{\mathrm{BP}} - t_{\mathrm{tr}}$ (Fig. 10), $t = (\pi - 0.5)/\omega_{\mathrm{BP}}$ (Fig. 11), $t = \pi/\omega_{\mathrm{BP}}$ (Fig. 12). These points correspond to the half-period of BP oscillations and characterise the processes of the WP transformations. The wave packet investigation at these times will allow us to establish the effect of beats on BP quantum oscillations.

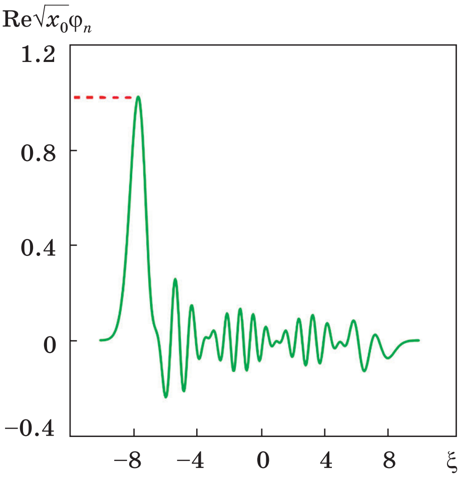

Fig. 12. The same as in Fig. 6, but for $t = \pi/\omega_{BP}$ [54]

Calculations show that in the point $t = 0.5/\omega_{BP}$, the WP is smeared (interaction with the right wall of the potential well decreases). After finishing of this process, at the moments of time $t \cong \omega_{BP}^{-1}$, it transforms into beats (Fig. 8). This wave, which is formed as a result of the superposition of two wave functions with equal amplitudes and close values of energies and wave numbers, provides the further transfer of quasiparticle energy.

After the transformation of the WP into beats, the train of the formed wave moves to the left wall of the well (see Figs. 9 and 10), near this wall, the reverse process of transforming beats into WP occurs at the moment of time $t = \pi/\omega_{BP} - t_{tr}$ (interaction with the left wall of the potential well increases). After this, the WP real part of the centre of gravity tends to localise near the left wall of the potential well of the oscillator (Figs. 11, *a*, 12), while the imaginary part of the WP goes to zero at the moment of time $t = \pi/\omega_{BP}$. Besides, the real part of the WP in the point $t = (\pi - 0.5)/\omega_{BP}$ coincides with one in the point $t = 0.5/\omega_{BP}$ (*cf*. Fig. 7, *a* with Fig. 11, *a*). In turn, the imaginary parts of the WP differ in sign (*cf*. Fig. 7, *b* with Fig. 11, *b*). In this case, the probability density of the quasiparticle $\varphi_n\varphi_n^*$ is equal. Future, after the moment of time $t = \pi/\omega_{BP}$, the process of BP quantum oscillations (the reverse movement of the WP to the right wall of the potential well) occurs in the order we indicated above.

Note also that the formation of a one-wave function train is caused by a single act of transformation of the WP in the point $t = t_{tr}$.

Let us find the group velocity of beats u_g, *i.e.*, the velocity of the maximum of their train. For this purpose, based on Ref. [73], we write down the expression for the beat amplitude b:

$$b = 2a_0 \left| \cos\left(\frac{1}{2}\left(t\frac{\Delta E}{\hbar} - \xi\Delta k \right) \right) \right|, \tag{31}$$

where a_0 is the amplitude of superposed wave functions, $\Delta E \ll E_{BP_n}$ and $\Delta k \ll k$ are small changes in their energy and wave number k, respectively.

Since only wave functions with $a_0 = \sqrt{x_0/2A_{BP_n}} = 0.254$ (and $k = \pi l x_0/A_{BP_n} = \pi l/7.7$, $l = 0,\ \pm 1,\ \pm 2 \ldots$) can propagate along the length $2A_{BP,n}/x_0$ (potential well width), we find $b_{max} = 2a_0 \approx 0.51$ (all parameters of the wave are given in the dimensionless form). In turn, the calculated results in Figs. 8–10 indicate that wave functions with $k = \pi/7.7$ ($l = 1$) superpose.

Obviously, the argument of the cosine in formula (31) is equal to π at the maximum point. Expanding it in series near a given point, we find $u_g = \dfrac{d\xi}{dt} = \dfrac{\Delta E}{\hbar\Delta k}$.

Substituting $dt \cong \pi/(2\omega_{BP}) - t_{tr}$ and $d\xi \approx A_{BP_n}/2x_0$ (Figs. 8 and 10) into this formula, we derive an expression for the average group velocity of beats, which in dimensional form can be written as

$$\langle u_g \rangle \approx 0.88\omega_{BP} A_{BP_n}. \tag{32}$$

At the same time, the average quasi-classical velocity of the oscillator is $(2/\pi)\omega_{BP}A_{BP_n} \approx 0.64\omega_{BP}A_{BP_n}$ within the range $-A_{BP_n} \le x \le A_{BP_n}$. This is less than $\langle u_g \rangle$, which is consistent with the fact that the beat train begins its motion at time t_{tr} and ends at $\pi/\omega_{BP} - t_{tr}$. Therefore, it needs a higher velocity to transfer the energy of the quasiparticle during a half-period of oscillation.

According to formula (32), the group velocity estimate for BP quantum oscillations in nickel and iron nanowires (for this WP) gives $\langle u_{g_{Ni}} \rangle \cong$ $\cong 1.8 \cdot 10^2$ cm/s and $\langle u_{g_{Fe}} \rangle \cong 5 \cdot 10^2$ cm/s, respectively. In this case, we have $t_{tr_{Ni}} \cong 5.3 \cdot 10^{-11}$ s and $t_{tr_{Fe}} \cong 2 \cdot 10^{-11}$ s.

Using relationship (26) and the group velocity values obtained above, one can estimate the μ_{BP}—mobility of the BP along the DW in the quasi-classical approximation according to the following formula $\mu_{BP} \propto \langle u_g \rangle / 8Mh_q$, where $h_{q_{Ni}} = 7.5 \cdot 10^{-3}$, $h_{q_{Fe}} = 16.1 \cdot 10^{-3}$ in our case $n = 30$. Thus, we have: $\mu_{BP_{Ni}} \approx 6$ cm·s^{-1}·Oe^{-1} and $\mu_{BP_{Ni}} \approx 2.5$ cm·s^{-1}·Oe^{-1}. Such values of BP mobility are significantly less than the same characteristic 76.4 cm·s^{-1}·Oe^{-1} in the yttrium garnet ferrite film [70] (this experiment was carried out at room temperature). Obviously, this fact is a consequence of the quantum dynamics of BP in the low-temperature region. In this case, the BP mobility along the DW can be measured practically, using SQUID magnetic techniques. In turn, the transformation time t_{tr} can be measured by radio-frequency spectroscopy methods [74].

7. Conclusion

The oscillatory properties of BP in the domain wall of a cylindrical FN are considered. The possibility of harmonic classical and quantum oscillations of BP is shown. The conditions of their practical realisation are established. The characteristic time of transformation of the BP wave packet into beats and back has been determined. This effect can be used as a basis for experimental techniques of detecting the process of BP quantum oscillations in cylindrical FN.

Authors' Contributions. A.B.Sh.: problem statement and solution, writing, methodology, investigation, analysis. A.V.M.: methodology, investigation, conceptualisation. O.V.O.: methodology, investigation, calculations, editing. M.Yu.B.: methodology, investigation, conceptualisation. All authors discussed the results, commented on the manuscript, contributed to its final version, and approved it.

REFERENCES

1. A.B. Shevchenko, Macroscopic quantum effects in domain boundaries of the uniaxial ferromagnetic films with the strong magnetic anisotropy, *Prog. Phys. Met.*, **19**, No. 2: 115 (2018);
https://doi.org/10.15407/ufm.19.02.115
2. W. Hong, S. Lee, H.J. Chang, E. S. Lee, and Y. Cho, Multifunctional magnetic nanowires: A novel breakthrough for ultrasensitive detection and isolation of rare cancer cells from non-metastatic early breast cancer patients using small volumes of blood, *Biomaterials*, **106**: 78 (2016);
https://doi.org/10.1016/j.biomaterials.2016.08.020
3. M.F. Contreras, R. Sougrat, A. Zaher, T. Ravasi, and J. Cosel, Non-chemotoxic induction of cancer cell death using magnetic nanowires, *Int. J. Nanomed.*, **10**: 2141 (2015);
https://doi.org/10.2147/IJN.S77081
4. W. Zhou, J. Um, Ya. Zhang, A. Nelson, Z. Nemati, J. Modiano, B. Stalder, and R. Franklin, Development of a biolabeling system using ferromagnetic nanowires, *IEEE J. Electromagnet., RF and Microwaves in Medicine and Biology*, **3**: 134 (2018);
https://doi.org/10.1109/JERM.2018.2889049
5. A.B.A. Nana, T. Marimuthu, P.P.D. Kondiah, Y.E. Choonara, L.C. DuToit, and V. Pillay, Multifunctional magnetic nanowires: design, fabrication, and future prospects as cancer therapeutics, *Cancers*, **11**: 1 (2019);
https://doi.org/10.3390/cancers11121956
6. D. Shore, A. Ghemes, O. Dragos-Pinzaru, Z. Gao, Qi Shao, A. Sharma, J. Um, I. Tabakovic, J.C. Bischof, and B.J.H. Stadler, Nanowarming using Au-tipped $Co_{35}Fe_{65}$ ferromafnetic nanowires, *Nanoscale*, **11**: 14607 (2019);
https://doi.org/10.1039/C9NR01182J
7. P.D. McGary, L. Tan, J. Zou, B. Stadler, P.R. Downey, and A.B. Flatau, Magnetic nanowires for acoustic sensors (invited), *J. Appl. Phys.*, **99**: 08B310 (2006);
https://doi.org/10.1063/1.2167332
8. S. Lepadatu, H. Saarikoski, R. Beacham, M. Jose-Benitez, T.A. Moore, G. Burnell, S. Sugimoto, D. Yesudas, M.C. Wheeler, J. Miguel, S.S. Dhessi, D. McGrouther, S. McVitie, G. Tatara, and C.H. Marrows, Synthetic ferrimagnet nanowires with very low critical current density for coupled domain wall motion, *Sci. Rep.*, **7**: 1640 (2017);
https://doi.org/10.1038/s41598-017-01748-7
9. S.S.P. Parkin, M. Hayashi, and L. Thomas, Magnetic domain-wall racetrack memory, *Science*, **320**: 190 (2008);
https://doi.org/10.1126/science.1145799
10. R. Zhu, S. Lilak, A. Loeffler, J. Lizier, A. Stieg, J. Gimzewski, and Z. Kuncic, Online dynamical learning and sequence memory with neuromorphic nanowire networks, *Nature Commun.*, **14**: 6697 (2023);
https://doi.org/10.1038/s41467-023-42470-5
11. E. Bruck, Handbook of Magnetic Materials: *Magnetic Nanowires and Nanotubes* (Netherlands: Elsevier: 2018).

12. *Handbook of Nanophysics: Nanotubes and Nanowires* (Ed. K.D. Sattler) (CRC Press: 2010);
https://doi.org/10.1201/9781420075434
13. A.B. Shevchenko and M.Yu. Barabash, Heat capacity of ferrite–garnet nanowire with domain wall, *Phys. B*, **556**: 114 (2019);
https://doi.org/10.1016/j.physb.2018.12.025
14. A.B. Shevchenko, M.Yu. Barabash, and I.M. Zabolotnyi, The effect of the domain wall on the entropy and the heat capacity of nickel nanowire, *Res. Phys.*, **16**: 102988 (2020);
https://doi.org/10.1016/j.rinp.2020.102988
15. A.B. Shevchenko, M.Yu. Barabash, O.V. Oliinyk, and O.V. Stepanov, Effect of thermal motion of transverse domain wall on thermodynamic states of cylindrical iron nanowire, *Res. Phys.*, **44**: 106133 (2023);
https://doi.org/10.1016/j.rinp.2022.106133
16. A.B. Shevchenko and M.Yu. Barabash, Magnetocaloric effect in nickel and iron nanowires with a domain wall, *Appl. Nanosci.*, **12**: 343 (2022);
https://doi.org/10.1007/s13204-020-01649-8
17. A.B. Shevchenko, M. Barabash, A. Minitskiy, and A. Kushko, *Magnetic Solitons in Extended Ferromagnetic Nanosystems Based on Iron and Nickel: Quantum, Thermodynamic, and Structural Effects* (SpringerBriefs in Materials: 2023);
https://doi.org/10.1007/978-3-031-40430-6
18. A. Hubert, *Theorie der Domänenwände in Geordneten Medien* (Berlin: Springer-Verlag: 1974) (in German).
19. C.A. Ferguson, D.A. MacLaren, and S. McVitie, Metastable magnetic domain walls in cylindrical nanowires, *J. Magn. Magn. Mater.*, **381**: 457 (2015);
https://doi.org/10.1016/j.jmmm.2015.01.027
20. R. Moreno, V.L. Carvalho-Santos, D. Altbir, and O. Chubykalo-Fesenko, Detailed examination of domain wall types, their widths and critical diameters in cylindrical magnetic nanowires, *J. Magn. Magn. Mater.*, **542**: 168495 (2022);
https://doi.org/10.1016/j.jmmm.2021.168495
21. A.B. Shevchenko and M.Yu. Barabash, Bloch point domain wall in cylindrical ferromagnetic nanowire, *Appl. Nanosci.*, **12**: 1747 (2022);
https://doi.org/10.1007/s13204-022-02397-7
22. A.P. Malozemoff and J.C. Slonczewski, *Magnetic Domain Walls in Bubble Materials* (New York: Academic Press: 1979).
23. V.F. Lisovskiy, *Fizika Tsilindricheskikh Magnitnykh Domenov* [Physics of Magnetic Bubblies] (Moskva: Soviet Radio: 1979) (in Russian).
24. R.G. Elías and A. Verga, Magnetization structure of a Bloch point singularity, *Eur. Phys. J. B*, **82**: 159 (2011);
https://doi.org/10.1140/epjb/e2011-20146-6
25. O.V. Pylypovskyi, D.D. Sheka, and Yu. Gaididei, Bloch point structure in a magnetic nanosphere. *Phys. Rev. B*, **85**, No. 22: 224401 (2012);
https://doi.org/10.1103/PhysRevB.85.224401
26. C. Andreas, A. Kákay, and R. Hertel, Multiscale and multimodel simulation of Bloch-point dynamics, *Phys. Rev. B*, **89**, No. 13: 134403 (2014);
https://doi.org/10.1103/PhysRevB.89.134403
27. S. Da Col, S. Jamet, N. Rougemaille, A. Locatelli, T.O. Mentes, B. Santos R. Burgos, M. Afid, L. Darques, J. Cagnon, C. Toussaint, and O. Fruchart, Observation of Bloch-point domain walls in cylindrical magnetic nanowires, *Phys. Rev. B*, **89**, No. 18: 180405(R), (2014);
https://doi.org/10.1103/PhysRevB.89.180405

28. R. Hertel, Ultrafast domain wall dynamics in magnetic nanotubes and nanowires. *J. Phys. Condens. Matter.*, **28**: 483002 (2016); https://doi.org/10.1088/0953-8984/28/48/483002
29. C. Donnelly, M. Guizar-Sicairos, V. Scagnoli, S. Gliga, M. Holler, J. Raabe, and L.J. Heyderman, Three-dimensional magnetization structures revealed with X-ray vector nanotomography, *Nature*, **547**: 328 (2017); https://doi.org/10.1038/nature23006
30. M.Y. Im, P. Fischer, K. Yamada, T. Sato, S. Kasai, Y. Nakatani, T. Ono, Symmetry breaking in the formation of magnetic vortex states in a permalloy nanodisk, *Nat. Commun.*, **3**: 983 (2012); https://doi.org/10.1038/ncomms1978
31. A. Wartelle, B. Trapp, M. Staňo, C. Thirion, S. Bochmann, J. Bachmann, M. Foerster, L. Aballe, T.O. Menteş, A. Locatelli, A. Sala, L. Cagnon, J.C. Toussaint, and O. Fruchart, Bloch-point-mediated topological transformations of magnetic domain walls in cylindrical nanowires, *Phys. Rev. B*, **99**, No. 2: 024433 (2019); https://doi.org/10.1103/PhysRevB.99.024433
32. M.Y. Im, H.S. Han, M.S. Jung, Y.S. Yu, S. Lee, S. Yoon, W. Chao, P. Fisher, J.I. Hong, and K. S. Lee, Dynamics of the Bloch point in an asymmetric permalloy disk, *Nat. Commun.*, **10**: 593 (2019); https://doi.org/10.1038/s41467-019-08327-6
33. X.P. Ma, J. Zheng, H.G. Piao, D.H. Kim, and P. Fisch, Cherenkov-type three-dimensional breakdown behavior of the Bloch-point domain wall motion in the cylindrical nanowire, *Appl. Phys. Lett.*, **117**, No. 6: 062402 (2020); https://doi.org/10.1063/5.0013002
34. M.T. Birch, D. Cortés-Ortuño, N.D. Khanh, S. Seki, A. Štefančič, G. Balakrishnan, and P.D. Hatton, Topological defect-mediated skyrmion annihilation in three dimensions, *Commun. Phys.*, **4**, No. 1: 175 (2021); https://doi.org/10.1038/s42005-021-00675-4
35. J.A. Fernandez-Roldan and O. Chubykalo-Fesenko, Dynamics of chiral domain walls under applied current in cylindrical magnetic nanowires, *APL Mater.*, **10**: 111101 (2022); https://doi.org/10.1063/5.0103408
36. G. Sáez, E. Saavedra, and N. Vidal-Silva, Dynamic susceptibility of a Bloch point singularity confined in a magnetic nanowire, *Res. Phys.*, **37**: 105530 (2022); https://doi.org/10.1016/j.rinp.2022.105530
37. M. Charilaou, Bloch point dynamics in exchange-spring heterostructures, *APL Matter.*, **10**, No. 7: 071103 (2022); https://doi.org/10.1063/5.0097610
38. M. Lang, M. Beg, O. Hovorka, and H. Fangohr, Bloch points in nanostrips, *Sci. Rep.*, **13**: 6910 (2023); https://doi.org/10.1038/s41598-023-33998-z
39. J. Hermosa, A. Hierro-Rodríguez, C. Quirós, J.I. Martin, A. Sorrentino, L. Aballe, E. Pereiro, M. Velez, and S. Ferrer, Bloch points and topological dipoles observed by X-ray vector magnetic tomography in a ferromagnetic microstructure, *Commun. Phys.*, **6**: 49 (2023); https://doi.org/10.1038/s42005-023-01162-8
40. J. Hermosa-Mucoz, A. Hierro-Rodríguez, A. Sorrentino, J.I. Martin, L.M. Alvarez-Prado, E. Pereiro, C. Quirós, M. Velez, and S. Ferrer, Hyperbolic Bloch points in ferrimagnetic exchange spring, *Res. Phys.*, **61**: 107771 (2024); https://doi.org/10.1016/j.rinp.2024.107771
41. E. Saavedra, F. Tejo, N. Vidal-Silva, and J. Escrig, Symmetry breaking-induced resonance dynamics in Bloch point nanospheres: unveiling magnetic volume effects

and geometric parameters for advanced applications in magnetic sensing and spintronics, *ACS Appl. Mater. Interfaces*, **16**, No. 21: 27605 (2024);
https://doi.org/10.1021/acsami.4c01963
42. A.B. Shevchenko and M.Yu. Barabash, Harmonic oscillation of point soliton (Bloch point) in cylindrical ferromagnetic nanowire, *Phys. B*, **668**: 415117 (2023);
https://doi.org/10.1016/j.physb.2023.415117
43. E.M. Chudnovsky, O. Iglesias, and P.C.E. Stamp, Quantum tunnelling of the domain walls in ferromagnets, *Phys. Rev. B*, **46**, No. 9: 5392 (1992);
https://journals.aps.org/prb/abstract/10.1103/PhysRevB.46.5392
44. A.B. Shevchenko, Quantum tunneling of a Bloch line in the domain wall of a cylindrical magnetic domain, *Tech. Phys.*, **52**, No. 10: 1376 (2007);
https://doi.org/10.1134/S1063784207100222
45. A.B. Shevchenko and M.Yu. Barabash, Quantum tunneling of the Bloch point in a magnetic film with strong uniaxial magnetic anisotropy, *Low Temp. Phys.*, **37**: No. 8: 690 (2011);
https://doi.org/10.1063/1.3660218
46. A.B. Shevchenko and M.Yu. Barabash, The over-barrier reflection of the Bloch point in uniaxial ferromagnets with strong magnetic anisotropy, *Low Temp. Phys.*, **39**: No. 2: 151 (2013);
https://doi.org/10.1063/1.4792131
47. A.B. Shevchenko and M.Yu. Barabash, The Bloch point in uniaxial ferromagnets as a quantum mechanical object, *Nanoscale Res. Lett.*, **9**: 132 (2014);
https://doi.org/10.1186/1556-276X-9-132
48. A.B. Shevchenko and M.Yu. Barabash, Quantum oscillations of the nanoscale structural inhomogeneties of the domain wall in magnetic bubble, *Nanoscale Res. Lett.*, **10**: 470 (2015);
https://doi.org/10.1186/s11671-015-1175-x
49. A.B. Shevchenko and M.Yu Barabash, Quantum oscillations of the interacting structural inhomogeneities of the domain wall in magnetic stripe domain, *Nanoscale Res. Lett.*, **11**: 473 (2016);
https://doi.org/10.1186/s11671-016-1680-6
50. A.B. Shevchenko and M.Yu. Barabash, Quantum oscillations of the Bloch point in the domain wall of the magnetic bubble, *Low Temp. Phys.*, **42**, No. 1: 42 (2016);
https://doi.org/10.1063/1.4940345
51. A.B. Shevchenko and M.Yu. Barabash, Quantum colliding of nanoscale solutions in a domain wall of magnetic stripe domain, *Appl. Nanosci.*, **9**: 595 (2019);
https://link.springer.com/article/10.1007/s13204-018-0644-9
52. A.B. Shevchenko and M.Yu. Barabash, One through the over tunnelling of the 'kink'-type solitons in domain wall of ferromagnetic film, *Res. Phys.*, **13**: 102294 (2019);
https://doi.org/10.1016/j.rinp.2019.102294
53. A. Tapia, C. Saji, A. Roldán-Molina, and A.S. Nunez, Stability enhancement by zero-point spin fluctuations: a quantum perspective on Bloch point topological singularities, *Advan. Funct. Mater.*, **34**, No. 32: 2312721 (2024);
https://doi.org/10.1002/adfm.202312721
54. A.B. Shevchenko, O.V. Oliinyk, A. Minitskyi, and M.Yu. Barabash, Quantum oscillations of Bloch point in cylindrical ferromagnetic nanowire: Quasiclassical approach, *Res. Phys.*, **73**, No. 6: 108245 (2025);
https://doi.org/10.1016/j.rinp.2025.108245
55. A.I. Akhiezer, V.G. Bar'yakhtar, and S.V. Peletminskii, *Spin Waves* (Amsterdam: North-Holland Publishing Company: 1968).

56. A.B. Shevchenko, M.Y. Barabash, A.B. Mel'nick, A.V. Minitskyi, and O.V. Oliinyk, Fractal approach to analysis of magnetic structure of domain wall with Bloch point in cylindrical ferromagnetic nanowire, *Nanooptics and Nanoelectronics, Nanobiotechnology, and Their Applications, NANO 2023*, *Springer Proc. Phys.*, **312**: 31 (2024) (Cham: Springer: 2024);
https://doi.org/10.1007/978-3-031-67527-0_3
57. A.B. Shevchenko and M.Yu. Barabash, A general formalism for the determination of the effective mass of the nanoscale structural inhomogeneities of the domain wall in uniaxial ferromagnets, *Nanoscale Res. Lett.*, **10**: 159 (2015);
https://doi.org/10.1186/s11671-015-0861-z
58. A.A. Thiele, Applications of the gyrocoupling vector and dissipation dyadic in the dynamics of the magnetic domains, *J. Appl. Phys.*, **45**: 377 (1974);
https://doi.org/10.1063/1.1662989
59. Yu.A. Kufaev and E.B. Sonin, Dynamics of a Bloch point (point soliton) in a ferromagnet, *Soviet Physics, JETP*, **68**: 879 (1989).
60. V.V. Batygin and I.N. Toptygin, *Sbornik Zadach po Ehlektrodinamike* [Problems in Electrodynamics] (Moskva: Nauka: 1970) (in Russian).
61. I.E. Tamm, *Fundamentals of the Theory of Electricity* (Moskva: Mir Publishers: 1979).
62. J.C. Slonczewski, Theory of domain wall motion in magnetic films and platelets, *J. Appl. Phys.*, **44**: 1759 (1973);
https://doi.org/10.1063/1.1662444
63. A.A. Thiele, Applications of the gyrocoupling vector and dissipation dyadic in the dynamics of the magnetic domains, *J. Appl. Phys.*, **45**: 377 (1974);
https://doi.org/10.1063/1.1662989
64. A.M. Fedorchenko, *Teoreticheskaya Fizika. Klassicheskaya Mekhanika* [Theoretical Physics. Classical Mechanics] (Kiev: Vyshcha Shkola: 1983) (in Russian).
65. L.D. Landay and E.M. Lifshitz, *Kvantovaya Mekhanika* [Quantum Mechanics] (Moskva: Nauka: 1989) (in Russian).
66. S.V. Vonsovskij, *Magnetizm* [Magnetism] (Moskva: Nauka: 1971) (in Russian).
67. L.D. Landay and E.M. Lifshitz, On the theory of the dispersion of magnetic permeability in ferromagnetic bodies, *Physikalische Zeitschrift der Sowjetunion*, **8**, No. 2: 153 (1935).
68. V.G. Bar'yakhtar, Phenomenological description of relaxation processes in magnetic materials, *Soviet Physics, JETP*, **60**, No. 4: 863 (1984).
69. E.G. Galkina, B.A. Ivanov, and V.A. Stephanovich, Phenomenological theory of Bloch point relaxation, *J. Magn. Magn. Mater.*, **118**, No. 3: 373 (1993);
https://doi.org/10.1016/0304-8853(93)90441-4
70. V.S. Gornakov, V.I. Nikitenko, and V.A. Prudnikov, Mobility of the Bloch point along the Bloch line, *JETP Lett.*, **50**, No. 11: 513 (1989).
71. C. Kittel, *Introduction to Solid State Physics* (New York: John Wiley Publishing: 1971).
72. A.A. Sokolov, Yu.M. Loskutov, and I.M. Ternov, *Kvantovaya Mekhanika* [Quantum Mechanics] (Moskva: Prosveshenie: 1965) (in Russian).
73. B.M. Yavorskiy and A.A. Detlaf, *Spravochnik po Fizike* [Reference Book in Physics] (Moskva: Nauka: 1985) (in Russian).
74. S. Svanberg, *Radio-Frequency Spectroscopy, Atomic and Molecular Spectroscopy: Basic Aspects and Practical Applications* (Berlin–Heidelberg: Springer-Verlag: 2004), Ch. 7, p. 187;
https://doi.org/10.1007/978-3-642-18520-5_7

Received / Final version
17.07.2025 / 19.01.2026

А.Б. Шевченко[1,2], *А.В. Мініцький*[3], *О.В. Олійник*[1], *М.Ю. Барабаш*[2,3]
[1] Інститут металофізики ім. Г.В. Курдюмова НАН України,
бульв. Академіка Вернадського, 36, 03142 Київ, Україна
[2] Технічний центр НАН України,
вул. Покровська, 13, 04070 Київ, Україна
[3] Національний технічний університет України
«Київський політехнічний інститут імені Ігоря Сікорського»,
просп. Берестейський, 37, 03056 Київ, Україна

БЛОХОВА ТОЧКА В ДОМЕННІЙ СТІНЦІ ЦИЛІНДРИЧНОГО ФЕРОМАГНЕТНОГО НАНОДРОТУ ЯК ГАРМОНІЧНИЙ ОСЦИЛЯТОР: КЛАСИЧНІ ТА КВАНТОВІ ВЛАСТИВОСТІ

Розглянуто коливні властивості (як класичні, так і квантові) блохової точки (БТ) у доменній стінці циліндричного феромагнетного нанодроту. На основі одержаних результатів зроблено висновок щодо можливості розгляду БТ як гармонічного осцилятора. Водночас квантові коливання БТ являють собою різновид магнетного макроскопічного квантового ефекту, який у випадку нікелевого та залізного нанодротів спостерігається в області гелієвих температур. Показано перетворення хвильового пакета БТ у процес биття, що забезпечує трансфер енергії квантового осцилятора. Наведені результати становлять особливий інтерес у контексті розвитку сучасних нанотехнологій, заснованих на фізичних властивостях циліндричних феромагнетних нанодротів, магнетна структура яких характеризується наявністю доменних стінок із БТ.

Ключові слова: циліндричний феромагнетний нанодріт, доменна стінка, блохова точка, гармонічні осциляції, хвильовий пакет, биття.